Mechanistic Pathways of the Hydroxyl Radical Reactions of Quinoline. 2. Computational Analysis of Hydroxyl Radical Attack at C Atoms

A. Roxana Nicolaescu,[†,‡,||] Olaf Wiest,*[,‡] and Prashant V. Kamat*[,†,§]

Radiation Laboratory, Department of Chemistry and Biochemistry, and Department of Chemical and Biomolecular Engineering, University of Notre Dame, Notre Dame, Indiana 46556-0579

Received: November 1, 2004; In Final Form: January 17, 2005

Density functional theory (DFT) calculations are employed to compare the mechanism of the •OH attacks at all carbon atoms in quinoline. The computational analysis of the energy surface for the reaction of •OH with quinoline reveals that the formation of OH adducts proceeds through exothermic formation of π-complexes/H-bonded complexes. The gas-phase reactions have activation energies ranging from <1.3 kcal/mol for the attack at positions C3 through C8 to 8.6 kcal/mol for the attack at the C2 position. Solvation, as described by the CPCM cavity model, lowers these activation barriers so that the attack at all carbon atoms except C2 is effectively barrierless. The •OH attack at C2 in solution is significantly different than at all other quinoline positions because it involves the only transition structure with energy higher than that of the starting materials and with an energetic barrier of 5.1 kcal/mol. The specific solvation approach also corroborates this finding because the attack at C2 was shown to have an energy barrier of 2.3 kcal/mol compared to the barrierless attack at C5. These results are in agreement with our recent experimental studies but differ from literature reports on the degradation of quinoline using the photo-Fenton reaction.

Introduction

In recent years, molecular modeling and computational chemistry have gained importance in the study of the molecular basis of environmental, chemical, and biological processes.[1−5] Computational studies offer a complementary approach to experimental studies and are used to gain greater insight into the reaction mechanisms. For example, they provide information on the energies, geometries, and electronic properties of the reactive intermediates and transition states that are not subject to direct observation in the •OH reactions.[6−10] Such theoretical studies[6,11−19] addressed the relative feasibility of the mechanisms postulated in the literature for the reaction of the hydroxyl radical with benzene and related systems.[20] There are also studies that assist in the identification of some radiation products by comparing experimental and theoretical results.[21−23]

Understanding the hydroxyl radical mechanisms is relevant to many scientific disciplines, and this is a very active field of research. Although there are studies in which •OH shows remarkable selectivity in its initial attack and this is reflected also in the analysis of steady-state products,[9] other studies suggest that it is the chemistry of the OH adducts that controls the outcome of the overall reaction. The formation of π complexes as precursors to OH adducts was suggested in various papers to explain the distribution of hydroxylated products in γ-radiolysis.[24,25] Van der Linde suggested that the formation of cyclohexadienyl-type radicals in many other substituted benzenes arises from the transition of the unlocalized OH adduct in the π complex to a localized position in the ring. The formation of these π complexes has been postulated in the radical reactions, which showed negative activation energies. However, there is little information regarding their structures and energies and their effect on the general mechanism of radicals with aromatic systems. Lundqvist and Eriksson reported the computed energy surface for the reaction of •OH with phenol at different levels of theory.[7] Two studies reported the transition-state energies of the OH adducts formed by addition at different positions of pyridine,[3,10] and another recent study reported on the structures of halogen atom−benzene π complexes.[26]

Density functional theory (DFT) methods have been tested extensively against highly correlated MO methods for the prediction of reliable geometries and reaction barriers.[3,27,28] Here, the B3LYP method with 6-31G* and 6-31+G* basis sets was used to study the reaction of quinoline with •OH radicals. The aim is to get a better understanding of the reaction mechanism and to clarify the discrepancies in the nature and distribution of hydroxylated products reported in the experimental studies described in the first part of this investigation.[29] In the radiolysis experiments, all of the hydroxylated products except one, 2-hydroxyquinoline/2-quinolinone, have been observed. In the photo-Fenton reactions, 7- and 3-hydroxyquinoline were not reported; 2- and 4-quinolinone were minor products, and only traces of 6-hydroxyquinoline were observed.[30] Because both experimental studies attribute the observed results to the reaction of the electrophilic hydroxyl radical with quinoline, computational analysis is used to further compare the reaction pathways of the •OH attack at all carbon atoms in quinoline. The relative stability of the final monohydroxylated quinolines has also been compared. The reaction energies (ZPE-corrected) for all possible addition adducts (OH adducts) and the energy barriers for their formation in the gas phase and using a polarizable conductor cavity model (CPCM)[31−33] to simulate the aqueous environment are presented in this study. Efforts have been made to investigate the effect of H-bonding on the reactivity at the C2 position. The H-bonding of the hydroxyl radical to the nitrogen atom

* Corresponding authors. E-mail: owiest@nd.edu, pkamat@nd.edu. Web: http://www.nd.edu/~pkamat.
† Notre Dame Radiation Laboratory.
‡ Department of Chemistry and Biochemistry.
§ Department of Chemical and Biomolecular Engineering.
|| E-mail: anicolae@hertz.rad.nd.edu.

10.1021/jp045016g CCC: $30.25
Published on Web 03/08/2005

SCHEME 1: Product Formation in the Reaction of •OH with Quinoline

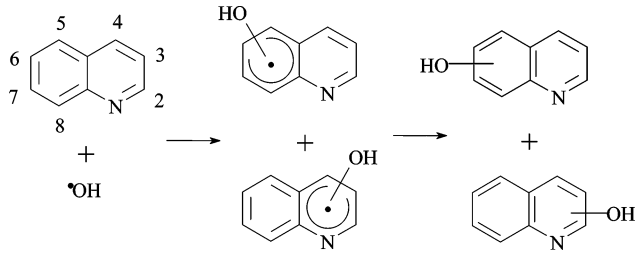

was prevented by including a water molecule in the picture and considering (quinoline··· H_2O) to be one of the reactants.

Computational Methodology

All geometry optimizations, harmonic vibrational frequencies, and zero-point energy calculations were performed with the B3LYP method with 6-31G* and 6-31+G* basis sets using the Gaussian 98 series of programs.[34] Gaussview was used to build the model structures to be optimized. Transition structures were characterized by harmonic frequency calculations, and all energies were corrected for zero-point vibrations. The reaction path was followed along the intrinsic reaction coordinate (IRC) from the transition structures to the reactant complexes to confirm their identity. The $\langle S^2 \rangle$ values ranged from a typical value of ~0.76 to a maximum value of ~0.79 before spin annihilation. The solvent effect was investigated by single-point calculations on the optimized gas-phase structures using the CPCM model[32,33] as implemented in Gaussian 98 with a dielectric constant of 78.39 for water. Standard values for the size of the cavity and the number of tesserae were used. The energies from these solvent calculations were also corrected by adding the zero-point energy corrections from the gas-phase frequency calculations. All energies are in kcal/mol, all bond lengths are in angstroms, unless otherwise specified, and all computations were done for 298.15 K and 1 atm.

Results and Discussion

Reaction Energies for the Formation of the Products. The reaction of •OH with quinoline involves first the formation of OH adducts with lifetimes on the order of microseconds.[35] These radical products then undergo transformations to the monohydroxylated quinolines. This is summarized in Scheme 1.

In the γ-radiolysis experiments described in the previous paper,[29] six of the possible seven monohydroxylated quinolines, viz., 3-, 4-, 5-, 6-, 7-, and 8-hydroxyquinolines, were confirmed as primary products of •OH reaction with quinoline. The first step in the computational analysis was to calculate the energy of all of the possible final hydroxylated products to determine their stability relative to each other. Interestingly, 2-hydroxyquinoline has been found to be the lowest-energy isomer, but it is the product not observed in the experiments. The energies of the final hydroxylated products, relative to the thermodynamically most stable product, 2-hydroxyquinoline, are presented in Table 1 for both the gas-phase and solution calculations. The effect of the solvent is reflected by a relatively small (<3 kcal/mol) stabilization in the energies of the products.

The next step in the computational approach was to determine the reaction energies (corrected for the zero-point energies) of the first step in Scheme 1, the formation of OH adducts. The attack of •OH on quinoline produces three energetically close rotamers for each possible hydroxy adduct except the one at C2 where only two rotamers were obtained. This is shown in Figure 1 for the attack at C8 and C2. The reaction energy (i.e., the difference between the energy of each C8 and, respectively, the C2 rotamer and reactants in the gas phase and using a solvent cavity model (CPCM) to model the aqueous environment) is presented in kcal/mol under each structure in Figure 1. The 8QOH-II isomer is the most stable in the gas phase. It is situated 24.2 kcal/mol below the reactants, as compared to 21.5 kcal/mol for 8QOH-I and 19.6 kcal/mol for 8QOH-III. However, 8QOH-I is the preferred conformer in solution. It is more stable than the starting materials by about 26 kcal/mol, compared to 23.7 kcal/mol in the case of 8QOH-II and 21.9 kcal/mol in the case of 8QOH-III. The 2QOH-I isomer is situated 18.5 kcal/mol below the reactants as compared to 19.3 kcal/mol for 2QOH-II in the gas phase. 2QOH-I is stabilized by solvation (CPCM) by only 1.1 kcal/mol, whereas the energy of 2QOH-II is not affected by the presence of the solvent. The difference between the energies of the two C2 rotamers in solution is very small, 0.4 kcal/mol. The relative energies of the different possible OH adducts with respect to the reactants were calculated at the B3LYP/6-31G* level both in the gas phase and in solution (CPCM model) for all possible rotamers (see Supporting Information). Only the results for the lowest-energy rotamers are presented in Table 2. For most isomers, the same trend in the stability of the rotamers was observed in the gas phase and in solution. The exceptions were the C2 and C8 isomers. This is most likely due to the stabilizing effect of the hydrogen bonding between the nitrogen of the quinoline and the hydrogen of the hydroxyl group in the gas phase.

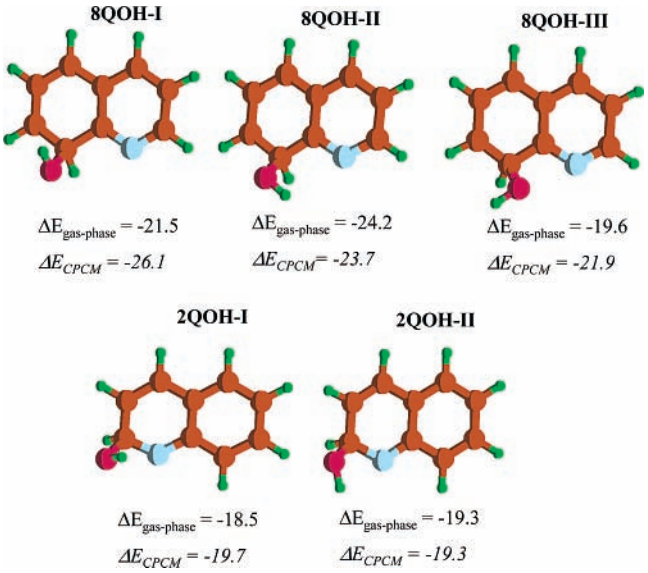

Figure 1. Possible rotamers formed by the attack of •OH at C8 and C2 and their energies (corrected for ZPE), in kcal/mol, in the gas phase and solution, relative to the reactants.

TABLE 1: B3LYP/6-31G* Energies of the Monohydroxylated Quinolines[a] in the Gas Phase and with the CPCM Model (kcal/mol)

isomers	Q2OH	Q3OH	Q4OH	Q5OH	Q6OH	Q7OH	Q8OH
gas phase	0	10.6	9.1	9.7	9.97	8.9	4.4
CPCM	0	8.1	7.0	7.4	7.3	6.5	6.1

[a] For example, Q2OH is 2-hydroxyquinoline.

The results of our calculations suggest that all of the addition reactions to either ring are energetically favorable, but there is no overwhelming energetic stability for any isomer as compared to the others. Moreover, the gas-phase and solution energies are quite similar, suggesting that solvent stabilization does not

TABLE 2: Reaction Energies for the OH-Adduct Formation[a] in the Gas Phase and with the CPCM Model (kcal/mol)

isomers		2QOH	3QOH	4QOH	5QOH	6QOH	7QOH	8QOH	
ΔE_{gas} phase	I	−18.5	−18.4	−21.7	−23.4	−18.5	−17.9	I	−21.5
	II	−19.3						II	−24.2
ΔE_{CPCM}	I	−19.7	−19.5	−22.1	−24.5	−19.3	−18.5	I	−26.1
	II	−19.3						II	−23.7

[a] For example, 2QOH is the 2-OH quinoline adduct.

play a major role in the case of OH adducts. The reaction energy values range from −17.9 to −24.3 kcal/mol for the formation of the OH adducts in the gas phase and from −18.5 to −26.1 kcal/mol in solution. The difference between the energies of the least stable and of the most stable isomer is about 7 kcal/mol. However, any two energetically adjacent isomers are separated at most by ∼2 kcal/mol or less. A similar trend can be observed for the thermodynamic stability of the OH adducts in both the gas phase and in solution: Q7OH < Q3OH, Q6OH < Q2OH < Q4OH < Q5OH < Q8OH. Although this is consistent with the experimentally observed lack of selectivity for attack at C3 through C8, it does not explain the absence of the C2-hydroxylated product. This demonstrates that the reaction cannot be understood on the basis of thermodynamics alone and that the OH adducts do not equilibrate. To obtain further insight, the reaction pathways in the gas phase and in solution were calculated on the time scale of the reaction.

Reaction Profiles for the Attack of •OH. Details of the mechanism for •OH attack at different positions in quinoline have been investigated further by locating the transition structures (TS) for the formation of OH adducts and the energy barriers for the attack at each position because the kinetic feasibility of the initial step may play an important role in explaining the outcome of this reaction. The energy profile for the attack of •OH at C5 and C2 to form the most stable conformers in the gas phase is shown in Figure 2A and B. The attack at C5 was chosen as representative of a reaction leading to an experimentally observed product to contrast with the C2 product that is not observed experimentally. The initial attack of the •OH radical at C5 is quite different than the attack at C2. In the first case, a π complex is formed. This π complex is more stable than the isolated reactants by 3.5 kcal/mol in the gas phase and by 1.5 kcal/mol in solution. The distance between C5 and the •OH radical is 2.44 Å. In the gas phase, the formation of the C5 OH adduct proceeds through a transition structure situated just barely above the π complex ($\Delta E = 0.3$ kcal/mol).

In solution, the transition-state energy is calculated to be lower than that of the π complex after the zero-point correction, implying a barrierless attack at C5. The transition-structure geometry, in which the distance between C5 and •OH is 2.17 Å, and energy closely resemble those of the π complex, indicating that the Hammond postulate is obeyed. In contrast, for the attack at C2, •OH interacts with quinoline by first forming a hydrogen bond with the nitrogen having a N−H bond length of 1.90 Å. The distance between the hydroxyl radical and C2 is 3.89 Å. In the gas phase, the H-bonded complex is 8.8 kcal/mol lower in energy than the starting materials and 8.6 kcal/mol below the C2 transition-state structure. In solution, the energy of the H-bonded complex is higher than in the gas phase by 4.8 kcal/mol but still below the energy of the isolated reactants by 4 kcal/mol. This energy is rapidly dissipated in solution, and the effective activation barrier is 5.1 kcal/mol. The transition-state search using the most stable C2 conformer in solution leads to the same transition state structure as presented earlier. For the attack at C2, the proximity of the nitrogen atom to C2 plays an important role. The considerable energetic cost for the attack at C2 versus the attack at C5 is due to the fact that N, which is the richest electronic site, steers the •OH radical in such a way that it first forms a planar hydrogen-bonded complex. For the C2 OH adduct to be formed, the hydrogen bond must be broken, and the •OH has to move from the plane of the quinoline molecule to its side, closer to C2. In addition, the C2 position has the lowest electron density of the seven potential sites of attack because of the electronegativity of the nitrogen. Thus, the transition structure for the attack of the electrophilic hydroxyl radical is the least favored at this position.

TABLE 3: Energies of the π-Complexes/H-Complexes and of Transition Structures Relative to the Isolated Species in the Gas Phase and with the CPCM Model (kcal/mol)

	gas phase		CPCM	
isomers (OH adducts)	π complex/H-complex (kca/mol)	TS (kcal/mol)	π complex/H-bonded complex (kca/mol)	TS (kcal/mol)
2QOH	−8.8	−0.2	−4.0	1.1
3QOH	−3.0	−2.2	−1.1	−1.8
4QOH	−3.0	−2.1	−1.1	−1.2
5QOH	−3.5	−3.3	−1.5	−2.3
6QOH	−3.5	−2.1	−1.5	−1.2
7QOH	−3.0	−1.7	−1.7	−1.3
8QOH	−3.0	−2.2	−1.7	−2.6
	(−8.8)	(−1.7)	(−4.0)	(−1.4)

In contrast to the attack at C2 and C5, two distinct energetic pathways were found for the attack of •OH at C8, and the structures and energies of the species involved are shown in Figure 3.

One pathway involves the formation of the H-bonded complex, similar to the one observed for the C2 attack, in which the distance between the hydroxyl radical and C8 is 3.36 Å (Figure 3B). In the gas phase, the effective activation barrier for this pathway is 7.1 kcal/mol. The energy barrier in solution is 2.6 kcal/mol, approximately half of the value calculated for the case of the attack at C2. The other pathway available for the hydroxyl radical attack at C8 resembles the reaction profile presented for C5. The formation of the π complex is favored by 2.9 kcal/mol in the gas phase and 1.8 kcal/mol in solution. The distance between C8 and •OH is 2.58 Å. The activation barrier is 0.75 kcal/mol in the gas phase. However, the energy of the solvated transition structure is lower than that of the solvated π complex, again implying a barrierless reaction in solution.

The calculated gas-phase and solution energy profiles for the attack of •OH at all of the C atoms in quinoline relative to the isolated reactants are presented in Table 3. The exothermic formation of a π complex is a common step for the attack at all positions except C2 and C8, in which case a very stable H-bonded complex is formed. The transition-structure energies in the gas phase are all situated above the energies of the π complexes. All of the solvated species have higher relative energies than in the gas phase, but in the case of the •OH attack at C3, C4, C5, and C8, the transition-state structures are energetically lower than the π complexes, indicating a barrierless process. Interestingly, the only species higher in energy than

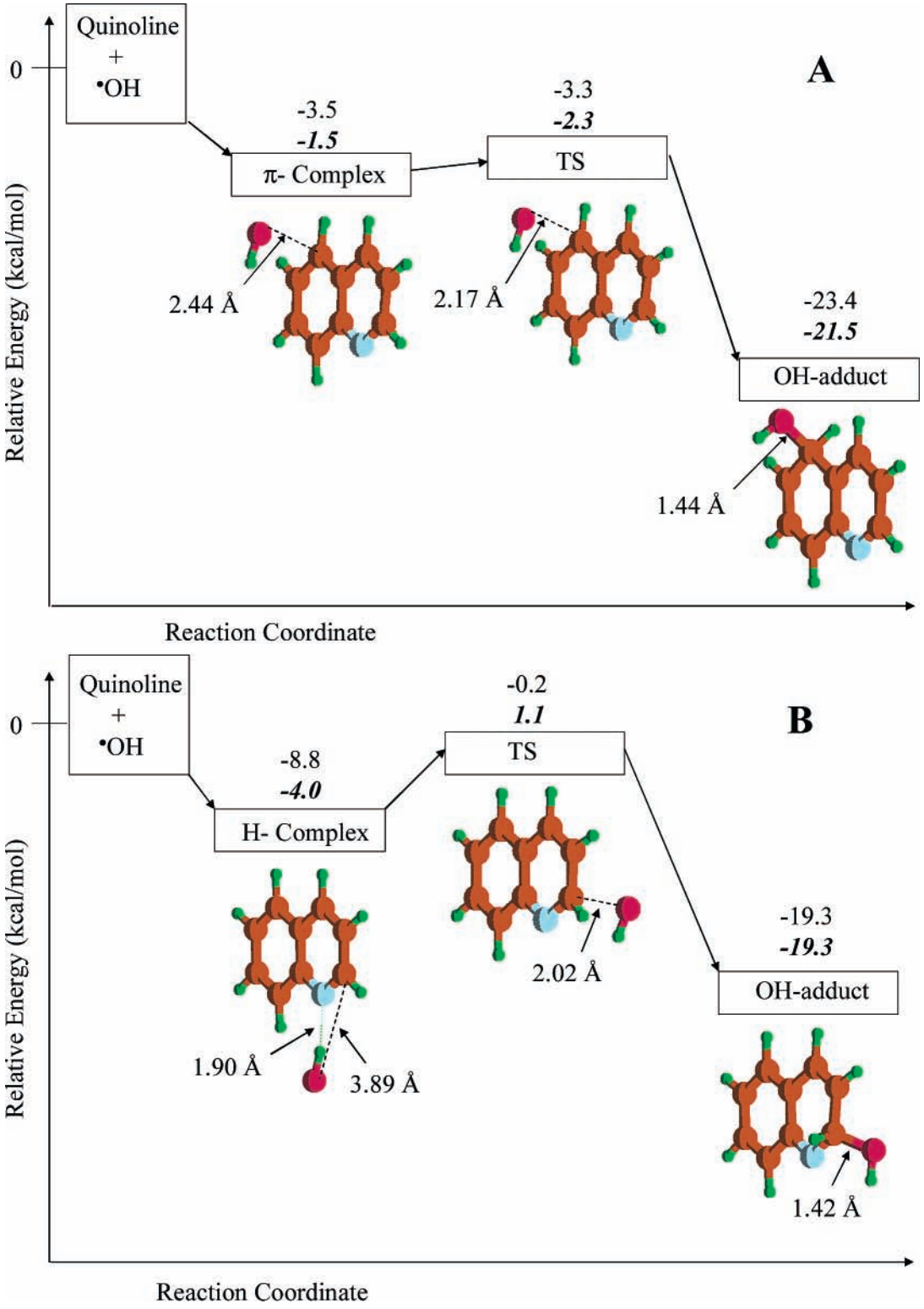

Figure 2. Reaction profile (ΔE + ZPE) for •OH addition at (A) C5 and (B) C2 at the B3LYP/6-31G* level. The energies (in kcal/mol) relative to the isolated reactants are shown for the gas phase and CPCM model (bold italics).

the reactants is the solvated transition state observed for the •OH reaction at C2. This correlates very well with the experimental results: the attack of •OH at C2 has the highest energetic cost and thus explains why 2-hydroxyquinoline is not observed in the reaction mixture.

The IRC calculations show that the π complexes are "shared": there are three π complexes formed for the attack at six carbon atoms. The reaction profile shows that the formation of C3 and C4 OH adducts proceeds through the same π complex. A similar situation is true for C5 and C6 and, respectively, for C7 and C8 OH adducts. This is consistent with an approximately equal interaction of the SOMO on the •OH with the π orbitals on the two carbon atoms. For the reaction at the benzene positions, it is observed that the formation of the most thermodynamically stable isomers (5QOH and 8QOH) in solution involves no activation energy according to the calculations with the CPCM model. There are energetic barriers for the reaction at C6 and C7, but they are very small: 0.3 and 0.4

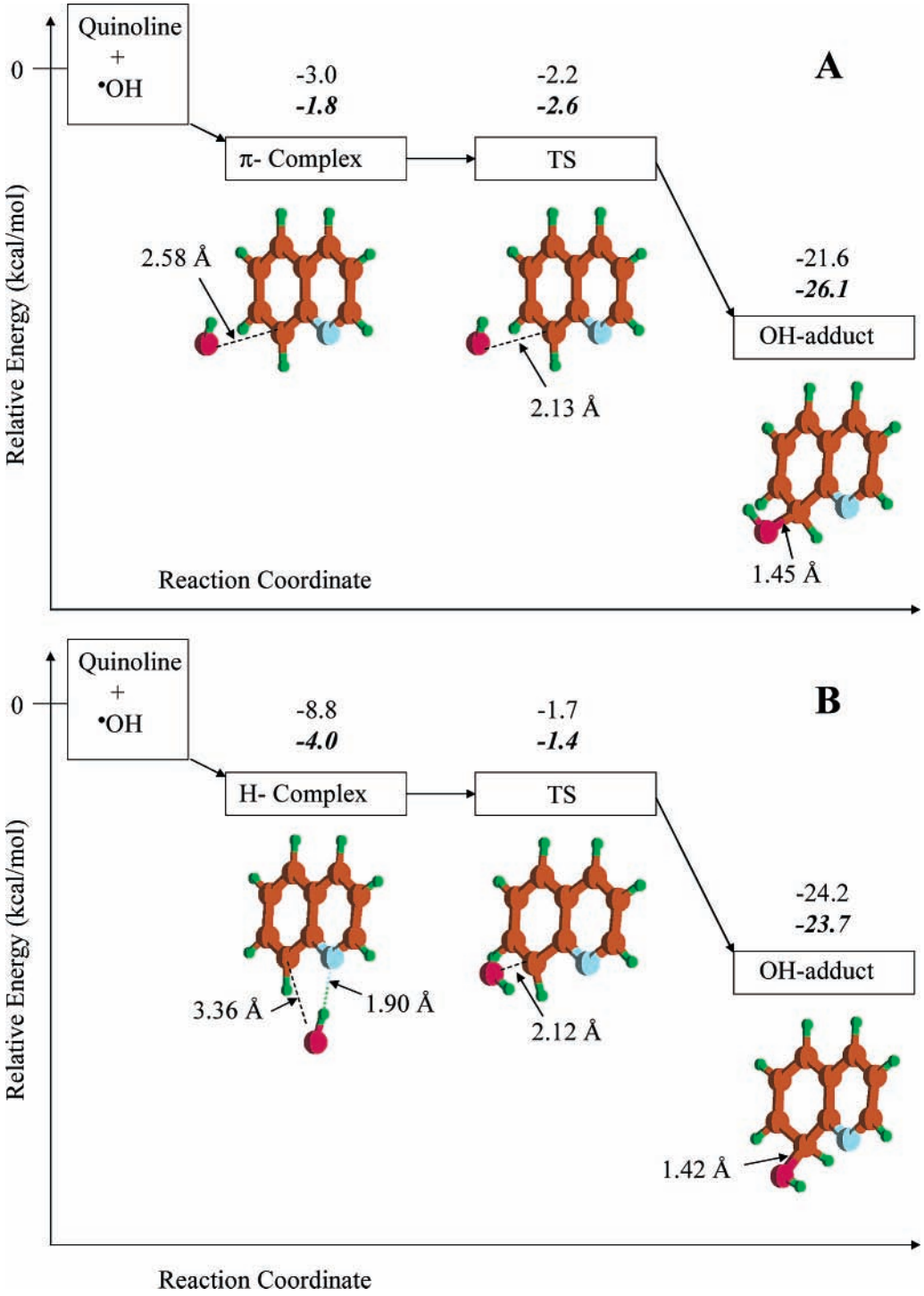

Figure 3. Reaction profile (ΔE + ZPE) for •OH addition at C8 (A) through a π complex and (B) through a H-bonded complex at the B3LYP/6-31G* level. The energies (in kcal/mol) relative to the isolated reactants are shown for the gas phase and CPCM model (italics).

kcal/mol. Therefore, these reactions can also be considered to be effectively barrierless.

Specific Solvation. Because the energetics for the attack of •OH at C2 and C8 was influenced by hydrogen bond formation between the nitrogen and •OH, the next step was to include a water molecule in our computations. Such an approach allows us explicitly to include the effect of the hydrogen bond between the hydroxyl radical and the nitrogen of quinoline in our study of the reaction profile. Such specific interactions are not represented in the cavity-type CPCM calculations discussed earlier in our study. In this case, the starting materials were the hydroxyl radical and quinoline−water. All of the calculations were done at the B3LYP/6-31+G* level.

The attack at C5 was investigated again, as it was considered to be a representative case for studying the effect of the added water molecule during the attack of •OH at all positions except C2 and C8. The energy profile is presented in Figure 4.

The energy calculations show that the transition structure is situated just below the π complex, which would suggest a barrierless attack at C5. However, the calculations of the free energy show a different picture, where the π complex is situated 3.9 kcal/mol above the reactants and there is a small barrier of ~1 kcal/mol to the transition structure due to the loss of entropy in the highly ordered transition structure.

In the case of the attack of •OH at C2, the transition-state structure was found, and then IRC (intrinsic reaction coordi-

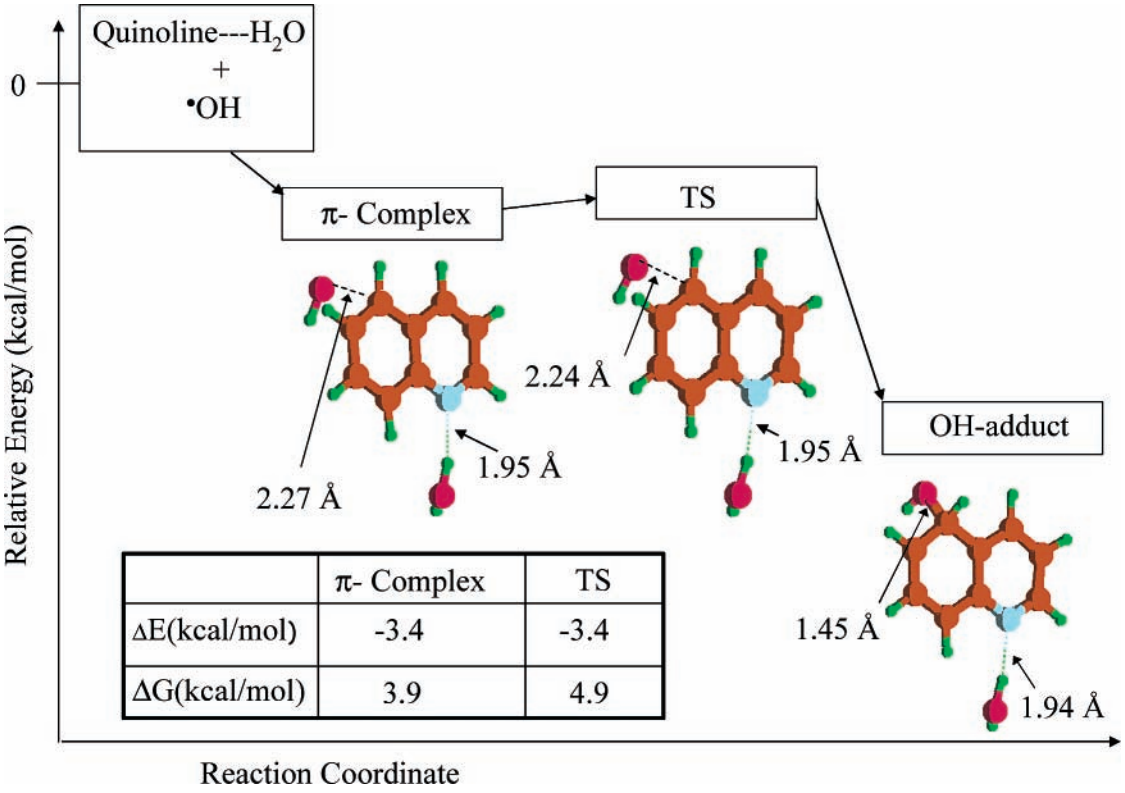

Figure 4. B3LYP/6-31+G* reaction profile for the hydroxyl radical attack at C5 including specific solvation. The energies, corrected for the ZPE, and free energies are shown relative to the isolated reactants.

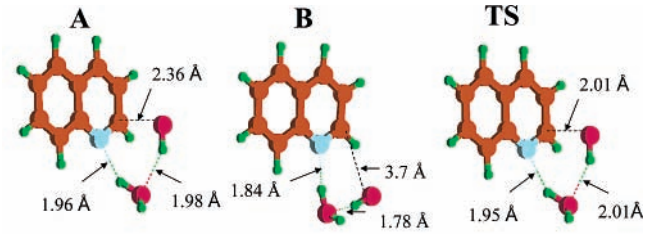

Figure 5. Geometries of (A) the IRC minimum, (B) the fully optimized minimum and, (TS) the transition structure calculated for the attack of the •OH radical on water-bound quinoline at C2.

nates) calculations were performed, which led to a very shallow minimum. When the structure obtained in the IRC calculations was optimized using tight geometry convergence criteria, there were significant changes in the geometry as well as the energy. This indicates that the barriers separating the shallow area located by the IRC calculations from a true minimum on the potential energy surface are very low. The geometries of the two minima and of the transition structure are presented in Figure 5.

The IRC minimum resembles both the transition structure and a π complex. The search for the lower-energy structure leads to the alignment of the water molecule in such a way that the N···HO angle is almost linear (172°); consequently, the •OH radical that is H-bonded to the water ends up being in the quinoline plane and quite far from the C2, as shown in Figure 5A. The energy barrier between the H-bonded complex and transition state is 7.7 kcal/mol, and the free-energy barrier is close to 9 kcal/mol. In the transition structure, the linearity of the H bonds characteristic of the lowest-energy geometry is disrupted as •OH moves toward C2. The hydrogen bonds in the transition structure (TS) are longer, similar to those shown in Figure 5A, and hence they are weaker that the H bonds in the H complex shown in Figure 5B. When the IRC minimum is considered, the transition-state energy barrier is 2.3 kcal/mol and the free-energy barrier is 3.3 kcal/mol. These activation energies are higher than those characteristic of the reaction of •OH to C5. A similar approach was used for the attack at the C8 position with the formation of the two conformers discussed earlier in the study (Supporting Information). In the case of the C8 rotamer that resembles the geometry of the attack at C2, the transition-state barrier for the IRC minimum is 0.6 kcal/mol, and the free-energy barrier is 2.1 kcal/mol. In the case of the other C8 rotamer, the transition-state barrier for the IRC minimum is only 0.04 kcal/mol, and the free-energy barrier is 1.1 kcal/mol. These values are very close to those obtained for the attack at C5 and support our approach using IRC minima with "loose optimization criteria" to get a "computational snapshot" of the •OH attack.

Conclusions

B3LYP calculations provide insight into the addition reaction of •OH at all quinoline positions. In the gas phase, the exothermic formation of a π complex is common for all quinoline positions except one. The attack at C2 involves the exothermic formation of a H-bonded complex. The transition structures are energetically situated below the starting materials and have activation barriers in the range of 8.6 kcal/mol for C2 to 0.2 kcal/mol for C5 attack. In solution, the reactions at C3, C4, C5, and C8 are barrierless as described by the CPCM model. The reactions at C6 and C7 show a very small energy barrier (0.3 and 0.4 kcal/mol) in solution, which indicates that these reactions are also feasible. The reactivity at C2 in solution is significantly different than at all other quinoline positions. The •OH attack at C2 involves the only TS with an energy higher than that of the starting materials and with a significant energetic barrier of 5.1 kcal/mol. This result agrees very well with the experimental studies presented in the previous paper (part 1)[29]

because 2-hydroxyquinoline is the only hydroxylated isomer not observed.

The combined results, experimental and computational, suggest that the nature of the products is determined in the initial addition step of the reaction of the hydroxyl radical with quinoline and that the chemistry of the OH adducts is relevant to the distribution of the final products. Moreover, the computational analysis implies a different mechanism for the formation of the products in the Fenton reaction[30] as compared to the direct attack of the hydroxyl radical, especially at C2.

Acknowledgment. We thank Dr. Ian Carmichael for the helpful discussions and all his suggestions. Special thanks to the ND Office of Information Technologies for the use of the computer facilities. This work was supported by the Office of Basic Energy Sciences of the U.S. Department of Energy. This is contribution no. NDRL-4564 from the Notre Dame Radiation Laboratory.

Supporting Information Available: The energies of the quinoline rotamers relative to the isolated reactants in the gas phase and with the CPCM model (B3LYP/6-31G*), an example of specific solvation attack at C8, and information regarding energies and free energies, ZPEs, Cartesian coordinates, and negative frequencies for the relevant species are presented. This material is available free of charge via the Internet at http://pubs.acs.org.

References and Notes

(1) Wolken, J. K.; Turecek, F. *J. Am. Chem. Soc.* **1999**, *121*, 6010−6018.

(2) Ghigo, G.; Tonachini, G. *J. Am. Chem. Soc.* **1999**, *121*, 8366−8372.

(3) Barckholtz, C.; Barckholtz, T. A.; Hadad, C. M. *J. Phys. Chem. A* **2001**, *105*, 140−152.

(4) Buda, F.; Ensing, B.; Gribnau, M. C. M.; Baerends, E. J. *Chem.—Eur. J.* **2001**, *7*, 2775−2783.

(5) Arnold, W. A.; Winget, P.; Cramer, C. J. *Environ. Sci. Technol.* **2002**, *36*, 3536−3541.

(6) Tokmakov, I. V.; Lin, M. C. *J. Phys. Chem. A* **2002**, *106*, 11309−11326.

(7) Lundqvist, M. J.; Eriksson, L. A. *J. Phys. Chem. B* **2000**, *104*, 848−855.

(8) Dibble, T. S. *J. Am. Chem. Soc.* **2001**, *123*, 4228−4234.

(9) Peller, J.; Wiest, O.; Kamat, P. V. *Chem.—Eur. J.* **2003**, *9*, 5379−5387.

(10) Vivekananda, S.; Wolken, J. K.; Turecek, F. *J. Phys. Chem. A* **2001**, *105*, 9130−9141.

(11) Andino, J. M.; Smith, J. N.; Flagan, R. C.; Goddard, W. A.; Seinfeld, J. H. *J. Phys. Chem.* **1996**, *100*, 10967−10980.

(12) Lay, T. H.; Bozzelli, J. W.; Seinfeld, J. H. *J. Phys. Chem.* **1996**, *100*, 6543−6554.

(13) Ghigo, G.; Tonachini, G. *J. Am. Chem. Soc.* **1998**, *120*, 6753−6757.

(14) Ghigo, G.; Tonachini, G. *J. Chem. Phys.* **1999**, *110*, 7298−7304.

(15) Molina, M. J.; Zhang, R.; Broekhuizen, K.; Lei, W.; Navarro, R.; Molina, L. T. *J. Am. Chem. Soc.* **1999**, *121*, 10225−10226.

(16) Bottoni, A.; Della Casa, P.; Poggi, G. *J. Mol. Struct.: THEOCHEM* **2001**, *542*, 123−137.

(17) Johnson, D.; Raoult, S.; Rayez, M. T.; Rayez, J. C.; Lesclaux, R. *Phys. Chem. Chem. Phys.* **2002**, *4*, 4678−4686.

(18) Motta, F.; Ghigo, G.; Tonachini, G. *J. Phys. Chem. A* **2002**, *106*, 4411−4422.

(19) Volkamer, R.; Klotz, B.; Barnes, I.; Imamura, T.; Wirtz, K.; Washida, N.; Becker, K. H.; Platt, U. *Phys. Chem. Chem. Phys.* **2002**, *4*, 1598−1610.

(20) Volkamer, R.; Platt, U.; Wirtz, K. *J. Phys. Chem. A* **2001**, *105*, 7865−7874.

(21) Ban, F. Q.; Gauld, J. W.; Boyd, R. J. *J. Phys. Chem. A* **2000**, *104*, 8583−8592.

(22) Ban, F. Q.; Gauld, J. W.; Boyd, R. J. *J. Phys. Chem. A* **2000**, *104*, 5080−5086.

(23) Schuler, R. H.; Albarran, G.; Zajicek, J.; George, M. V.; Fessenden, R. W.; Carmichael, I. *J. Phys. Chem. A* **2002**, *106*, 12178−12183.

(24) Volkert, O.; Schulte-Frohlinde, D. *Tetrahedron Lett.* **1968**, *17*, 2151−2154.

(25) Ashton, L.; Buxton, G. V.; Stuart, C. R. *J. Chem. Soc., Faraday Trans.* **1995**, *91*, 1631−1633.

(26) Tsao, M. L.; Hadad, C. M.; Platz, M. S. *J. Am. Chem. Soc.* **2003**, *125*, 8390−8399.

(27) Curtiss, L. A.; Redfern, P. C.; Raghavachari, K.; Pople, J. A. *J. Chem. Phys.* **2001**, *114*, 108−117.

(28) Lynch, B. J.; Truhlar, D. G. *J. Phys. Chem. A* **2001**, *105*, 2936−2941.

(29) Nicolaescu, A. R.; Wiest, O.; Kamat, P. V. *J. Phys. Chem. A* **2005**, *109*, 2822.

(30) Cermenati, L.; Pichat, P.; Guillard, C.; Albini, A. *J. Phys. Chem. B* **1997**, *101*, 2650−2658.

(31) Barone, V.; Cossi, M. *J. Phys. Chem. A* **1998**, *102*, 1995−2001.

(32) Barone, V.; Cossi, M.; Tomasi, J. *J. Comput. Chem.* **1998**, *19*, 404−417.

(33) Cossi, M.; Barone, V. *J. Chem. Phys.* **1998**, *109*, 6246−6254.

(34) Frisch, M. J.; Trucks, G. W.; Schlegel, H. B.; Scuseria, G. E.; Robb, M. A.; Cheeseman, J. R.; Zakrzewski, V. G.; Montgomery, J. A., Jr.; Stratmann, R. E.; Burant, J. C.; Dapprich, S.; Millam, J. M.; Daniels, A. D.; Kudin, K. N.; Strain, M. C.; Farkas, O.; Tomasi, J.; Barone, V.; Cossi, M.; Cammi, R.; Mennucci, B.; Pomelli, C.; Adamo, C.; Clifford, S.; Ochterski, J.; Petersson, G. A.; Ayala, P. Y.; Cui, Q.; Morokuma, K.; Malick, D. K.; Rabuck, A. D.; Raghavachari, K.; Foresman, J. B.; Cioslowski, J.; Ortiz, J. V.; Stefanov, B. B.; Liu, G.; Liashenko, A.; Piskorz, P.; Komaromi, I.; Gomperts, R.; Martin, R. L.; Fox, D. J.; Keith, T.; Al-Laham, M. A.; Peng, C. Y.; Nanayakkara, A.; Gonzalez, C.; Challacombe, M.; Gill, P. M. W.; Johnson, B. G.; Chen, W.; Wong, M. W.; Andres, J. L.; Head-Gordon, M.; Replogle, E. S.; Pople, J. A. *Gaussian 98*, revision A.9; Gaussian, Inc.: Pittsburgh, PA, 1998.

(35) Nicolaescu, A. R.; Wiest, O.; Kamat, P. V. *J. Phys. Chem. A* **2003**, *107*, 427−433.